

## Supporting Information

### Laser irradiated vortex fluidic mediated synthesis of luminescent carbon nanodots under continuous flow

Xuan Luo<sup>1,2</sup>, Ahmed Hussein Mohammed Al-Antaki<sup>2</sup>, Kasturi Vimalanathan<sup>2</sup>, Jillian Moffatt,<sup>3</sup> Kun  
Zheng<sup>4,5</sup>, Yichao Zou<sup>6</sup>, Jin Zou<sup>4,6</sup>, Xiaofei Duan<sup>7</sup>, Robert N. Lamb<sup>8</sup>, Shujun Wang<sup>9</sup>, Qin Li<sup>9</sup>, Wei Zhang<sup>1\*</sup>  
and Colin L. Raston<sup>2\*</sup>

<sup>1</sup> Centre for Marine Bioproducts Development, College of Medicine and Public Health, Flinders University,  
Adelaide, SA 5042, Australia;

<sup>2</sup> Centre for NanoScale Science and Technology (CNST), College of Science and Engineering, Flinders University,  
Adelaide, SA 5042, Australia;

<sup>3</sup> Institute for Photonics and Advanced Sensing, and School of Physical Sciences, The University of Adelaide, SA  
5005, Australia;

<sup>4</sup> Centre for Microscopy and Microanalysis, The University of Queensland, Brisbane, QLD 4072, Australia;

<sup>5</sup> Australian Institute for Bioengineering and Nanotechnology, The University of Queensland, Brisbane, QLD 4072,  
Australia;

<sup>6</sup> Materials Engineering, The University of Queensland, Brisbane, QLD 4072, Australia;

<sup>7</sup> Trace Analysis for Chemical, Earth and Environmental Sciences (TrACEES), The University of Melbourne, Victoria  
3010, Australia;

<sup>8</sup> School of Chemistry, The University of Melbourne, Victoria 3010, Australia;

<sup>9</sup> Environmental Engineering and Queensland Micro and Nanotechnology Centre, Griffith University, Brisbane,  
QLD 4111, Australia.

#### Corresponding Authors

\*C. Raston. Tel.: +61 8 82017958. Fax: +61 8 8201290. E-mail: [colin.raston@flinders.edu.au](mailto:colin.raston@flinders.edu.au)

\*W. Zhang. Tel.: +61 8 72218557. Fax: +61 8 72218555. E-mail: [wei.zhang@flinders.edu.au](mailto:wei.zhang@flinders.edu.au)

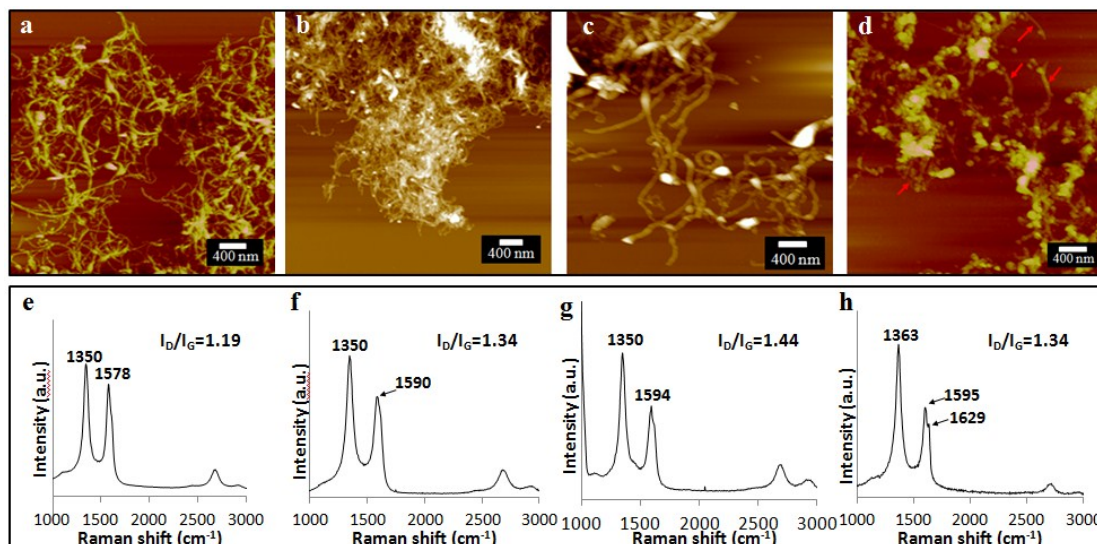


**Fig. S1** AFM images of MWCNTs. (a) As received MWCNTs. (b) MWCNTs dispersed using the magnetic-assisted syringe for 2 h. (c) MWCNTs at a concentration of 0.5 mg/mL processed in the VFD at 7500 rpm without laser irradiation. (d) MWCNTs laser irradiated at 460 mJ for 9 minutes (equivalent to the retention time of VFD under the optimized conditions) in a quartz cuvette with magnetic stirrer without VFD treatment. Red arrows indicate the presence of MWCNTs. (e-h) Raman spectra of samples as shown in the AFM images a-d, respectively.

Under continuous flow processing, 45 mL of dispersed solution of MWCNTs in a syringe pump was delivered over 1.67 h into the VFD with the tube rotating at 7500 rpm (flow rate of 0.45 mL/min). A G band shoulder was observed at 1629 cm<sup>-1</sup> when decoupling VFD processing from the irradiation with the laser (Fig. S1h), which represents induced structural disorder.<sup>1</sup> In contrast, the high mass transfer in the VFD dissipates the heat, and thus the breakdown of MWCNTs is more controlled as evidenced by highly ordered G bands (Fig. S1g).

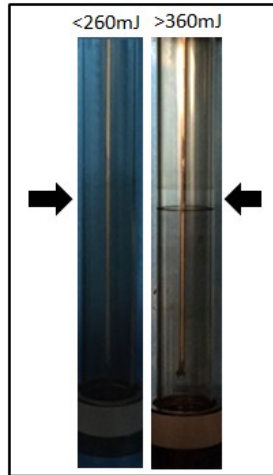


**Fig. S2** Photograph showing the band formed at the irradiation site when the laser power was  $> 360$  mJ, and absent when  $< 260$  mJ.

The optimized laser power was between 360 to 460 mJ (Fig. 3) with a clear band observed in the tube where the 8 mm diameter laser beam irradiated the glass tube (Fig. S2), as for slicing of CNTs.<sup>2</sup>

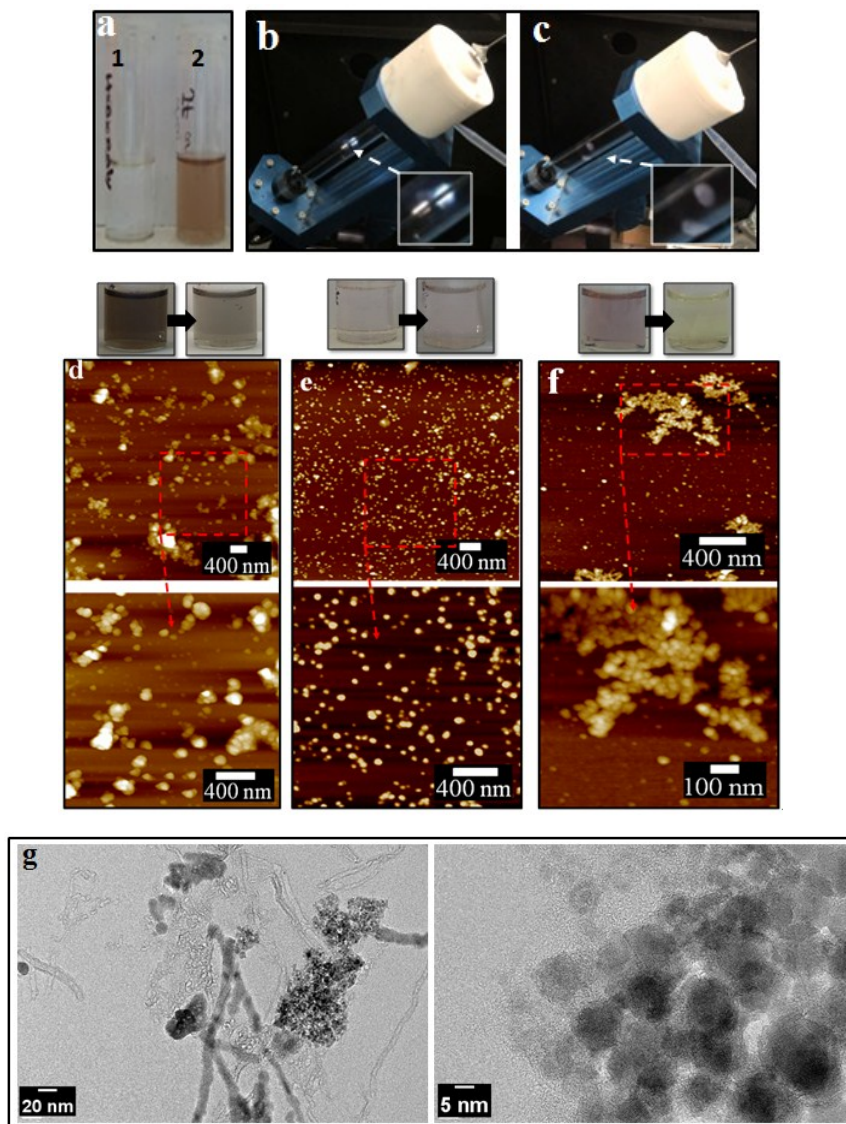


**Fig. S3.** Products formed when the laser is directed towards the stainless steel jet feed. (a) Laser processing of aqueous H<sub>2</sub>O<sub>2</sub> in the absence of MWCNTs. 1: Laser not irradiating the jet feed. 2: Laser irradiating the jet feed. (b) Laser irradiating the jet feed. (c) Laser not irradiating the jet feed. (d) AFM images of processed MWCNTs at a concentration of 0.5 mg/mL with the jet feeds positioned to avoid laser beam exposure. (e) AFM images of H<sub>2</sub>O<sub>2</sub> processed with laser irradiating the jet feed. (f) AFM images of processed MWCNTs at a concentration of 0.5 mg/mL with laser irradiating the jet feed. All experiments were conducted in laser-assisted VFD processing under continuous flow at 0.45 mL/min at 7500 rpm with the pulsed laser operating at 450 mJ. (g) TEM images of CDs contaminated by metal oxide nanoparticles resulting from the laser irradiating the stainless steel jet feed.

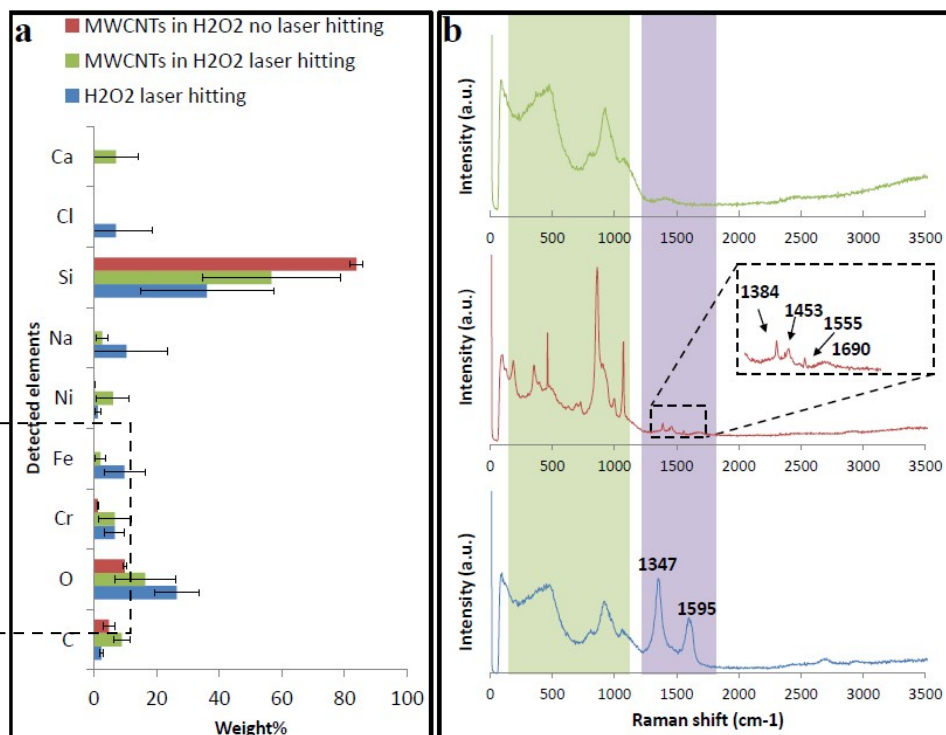


**Fig. S4** Effect of the laser irradiating the stainless steel jet feed. (a) SEM/EDX of as processed samples with or without laser irradiation. (b) Raman spectra of an empty glass tube, H<sub>2</sub>O<sub>2</sub> with the laser irradiating the jet feed and MWCNTs in H<sub>2</sub>O<sub>2</sub> with the laser beam irradiating the jet feed, respectively.

After being processed at or above the laser power of 350 mJ, the as processed liquid was purple which turned yellow after four days at room temperature. The control experiment of H<sub>2</sub>O<sub>2</sub> alone processed at 7500 rpm at a laser power of 450 mJ (laser irradiating the jet feed) generated nanoparticles. SEM/EDX on these samples showed the presence of iron, chromium and nickel which was not detected in the as received MWCNTs (Fig. S4a).

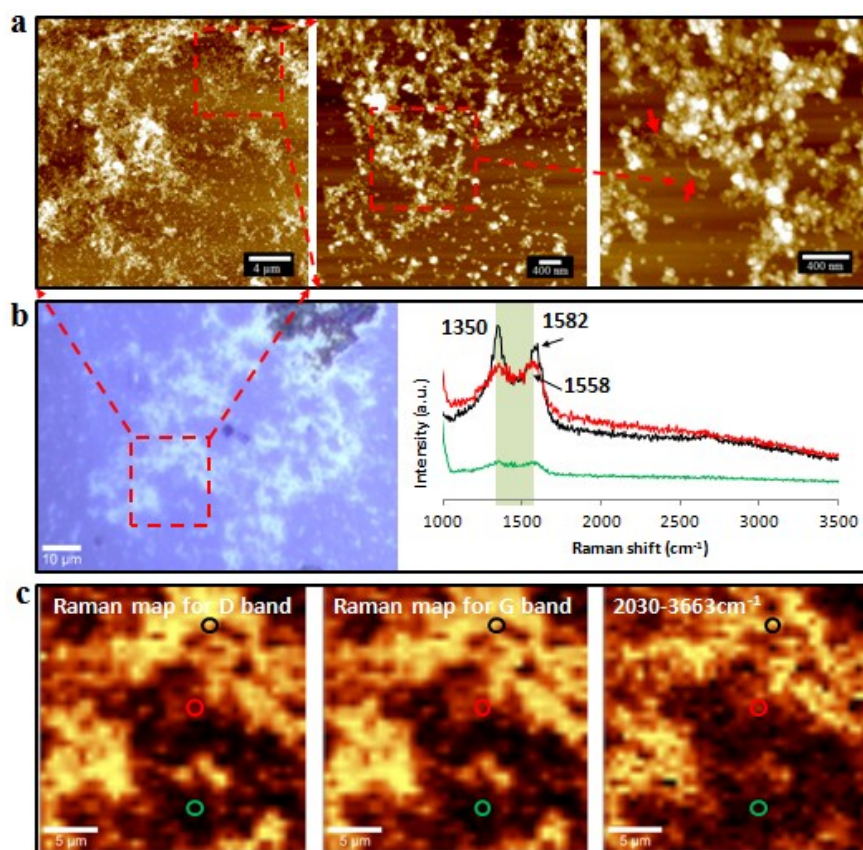


**Fig. S5.** Raman mapping for MWCNTs dispersed in H<sub>2</sub>O<sub>2</sub> at 0.5 mg/mL, processed at 240 mJ and avoiding the laser irradiating the jet feed. (a) AFM of the mapped area. (b) Optical images of the mapped area (highlighted in the red square). (c) Raman mapping of the D band (1350 cm<sup>-1</sup>), G band (1582 cm<sup>-1</sup>) and the broad fluorescence band (2030-3663 cm<sup>-1</sup>) from left to right. Scanned area was 20 × 20 μm<sup>2</sup>.

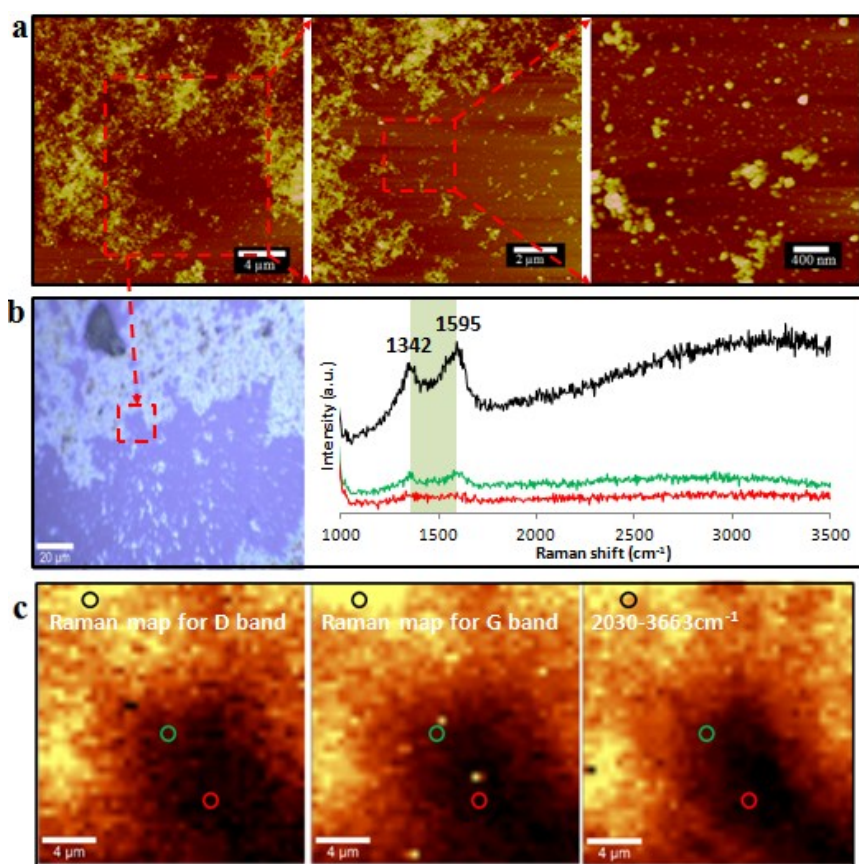


**Fig. S6.** Raman map of CDs fabricated under continuous flow VFD processing (0.5 mg/mL, 0.45 mL/min, 7500 rpm) while irradiated with a pulsed laser (1064 nm, 450 mJ) at 45° tilt. (a) AFM images of the mapped area. (b) Optical images of the mapped area (highlighted in the red square) and three representative Raman spectra circled in (c) mapping the D band (1342  $\text{cm}^{-1}$ ), G band (1595  $\text{cm}^{-1}$ ) and a broad band (2030  $\text{cm}^{-1}$ -3663  $\text{cm}^{-1}$ ) from left to right, respectively. Scanned area was  $20 \times 20 \mu\text{m}^2$ .

Raman mapping was used to verify the crystalline nature and degree of  $sp^2$  hybridisation of the CDs relative to the MWCNTs, prepared under two different laser wavelength. From AFM images, CDs prepared using a NIR laser (Fig. S6a) were more homogeneous than for the laser operating at 532 nm, which revealed short nanotubes (Fig. S5a). Raman maps on these areas are consistent with result from AFM studies. Three maps corresponding to D (1352  $\text{cm}^{-1}$ ) band, G (1594  $\text{cm}^{-1}$ ) band and a broad band from 3020 to 3663  $\text{cm}^{-1}$  were obtained (Fig. S5c and S6c). All the mapping results established the presence of graphitic materials with well-matched signals for D and G bands. Single Raman spectrum (Fig. 5b and 6b) extracted from three randomly circled areas showed typical graphitic spectrum but processing with the laser operating at 532 nm (Fig. S5, Table S1) showed lower CD formation and poorer sample homogeneity relative to those prepared using a NIR laser ( $\theta$  45°, 7500 rpm rotational speed) operating at 1064 nm (Fig. S6). In addition, a significant increase in the background intensity was evident for the CDs obtained from NIR laser (Fig. S6b) which implies fluorescence emission under Raman laser excitation at 532 nm.<sup>3</sup>

**Table S1.** Raman shift ( $\text{cm}^{-1}$ ) of the as-received MWCNTs and the one processed with green laser (532 nm) or NIR laser (1064 nm) with one or two cycles of laser-VFD processing. 50 single spectra for each sample were analysed and averaged.

	D band	G band	$I_D/I_G$
As received	1346±3.1	1586±8.3	1.19±0.07
Green light	1357±5.0	1578±8.5	1.03±0.05
NIR 1 <sup>st</sup> VFD cycle	1354±5.2	1588±7.1	0.96±0.11
NIR 2 <sup>nd</sup> VFD cycle	1352±5.7	1594±6.1	0.99±0.03
NIR 1 <sup>st</sup> VFD cycle pellet	1352.39±6.5	1591±9	1.34±0.21

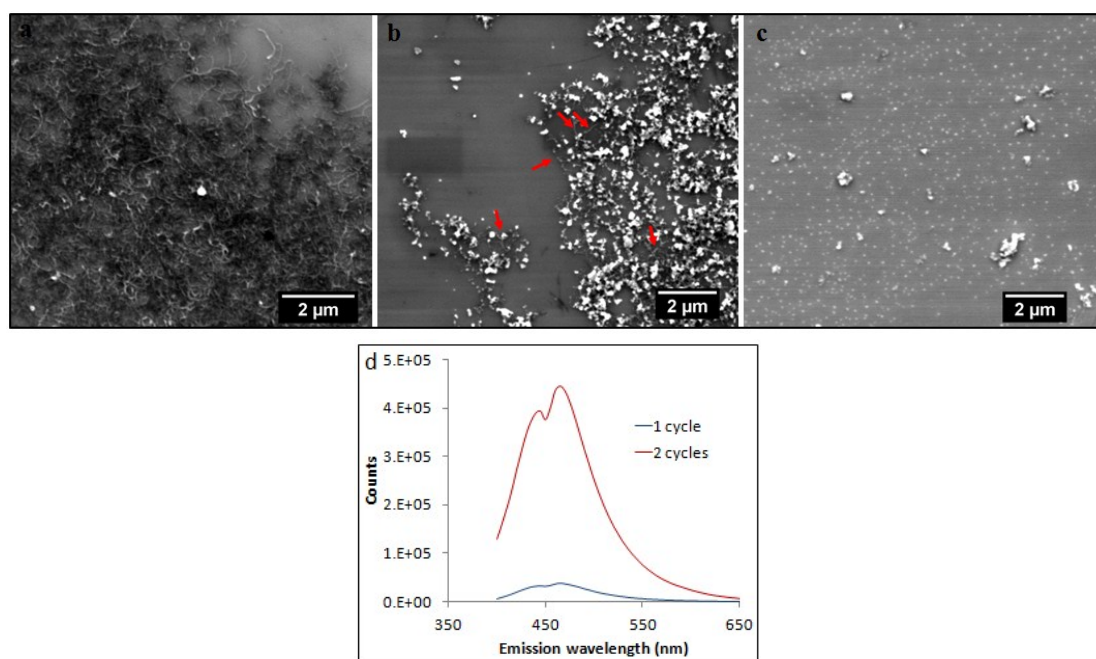


**Fig. S7** SEM of (a) as received MWCNTs at 0.1 mg/mL. (b) 0.1 mg/mL MWCNTs processed at a flow rate of 0.45 mL/min at 45° tilt, 7500 rpm with laser power at 460 mJ. (c) 0.1 mg/mL MWCNTs processed twice in the VFD using the same condition as in (b). The as-processed sample was directly drop-casted on a silicon wafer before imaging without centrifugation. (d) Photoluminescence of one cycle and two cycles processed CDs under the optimized condition.

Even though the conversion rate was considered to be the highest at 0.1 mg/mL, approximately 20% debundled CNTs were still evident under SEM while investigating the entire wafer surface (Fig. S7b). Photoluminescence is one of the classic signatures of CDs and their intensity largely depends on the sample concentration.<sup>4</sup> The twice laser-VFD cycle processed sample showed a much higher intensity (11.8 times) than one cycle process one.

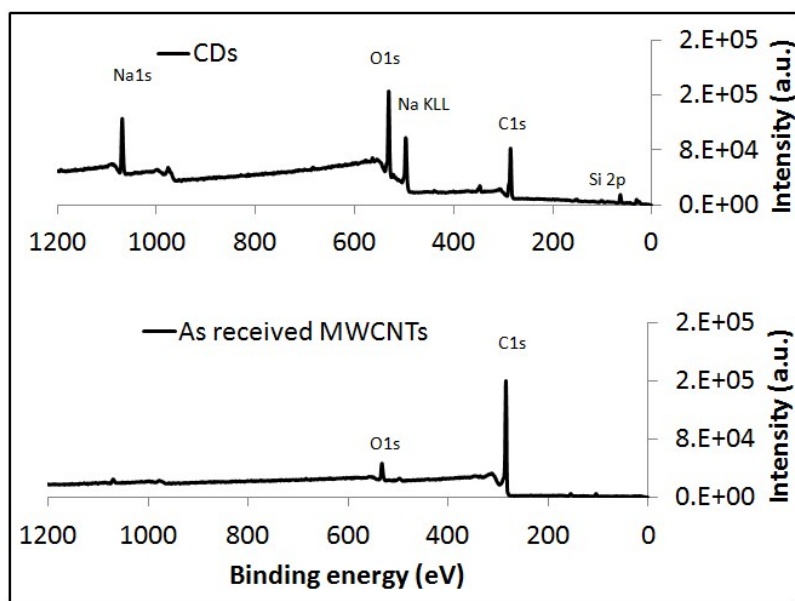


Fig. S8 XPS full profile of the as-received MWCNTs and CDs fabricated under optimized conditions.

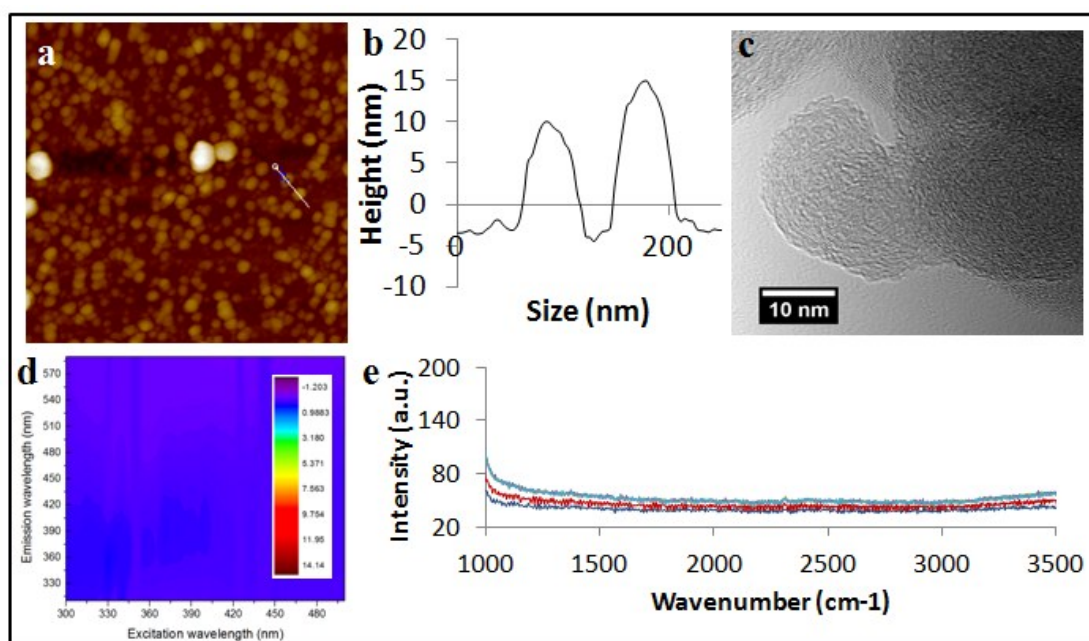


Fig. S9 Non-graphitic nanoparticles observed for intensively washed as-received MWCNTs multiple times (MilliQ water). The supernatant was drop-casted for characterization: (a) AFM. (b) height plot (c) HRTEM. (d) 2D Fluorescence map, and (e) Raman spectrum

As-received MWCNTs were intensively washed with MilliQ water multiple times and the supernatant were used for characterization. As shown, non-crystalline and non-graphitic nanoparticles with height at about 20 nm showed no fluorescence in a 2D fluorescence map.

The quantum yield was calculated according to:

$$\Phi_S = \Phi_{ST} \left( \frac{m_S}{m_{ST}} \right) \left( \frac{\eta_S}{\eta_{ST}} \right)^2$$

Where  $\Phi_S$  is the relative quantum yield with respect to the reference anthracene.  $m_{ST}$  and  $m_S$  are from the calibration curves obtained below.  $\eta_{ST}$  and  $\eta_S$  are the refractive indexes of the solvent.

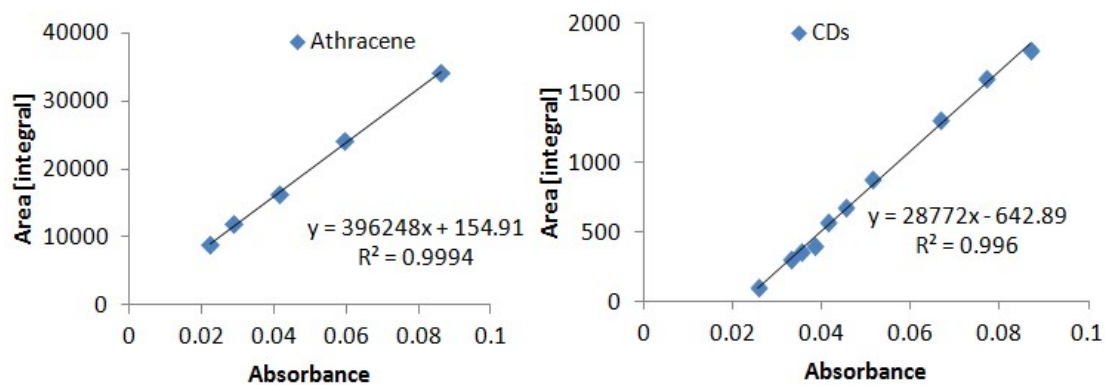


**Table S2.** Quantum yield calculation of CDs fabricated under optimized conditions.

Sample	Quantum yield ( $\Phi$ )	m from calibration curves	Refractive index of solvent ( $\eta$ )
Anthracene	30% (known)	396248	1.33
CDs	2.2%	28772	1.33

**Table S3:** The UV diodes peak wavelength and the corresponding spectra width and power for photoluminescence (Edinburgh Instruments F980 Spectrofluorimeter)

Diodes peak wavelength (nm)	Spectra width (nm)	Power ( $\mu\text{W}$ )	Part number
276.7	10.8	657	UVTOP270TO39HS
286.8	10.9	883	UVTOP285TO39HS
298.3	10.4	451	UVTOP295TO39HS
314.9	10.6	538	UVTOP310TO39HS
355	15	300	UVLED355TO46FW

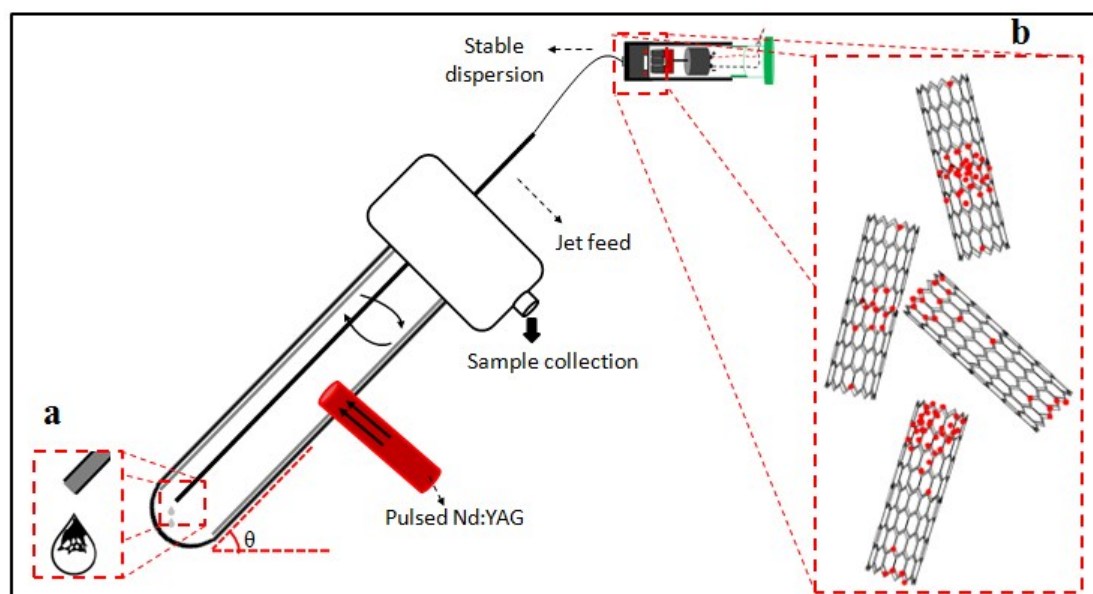


**Fig. S10.** Proposed fabrication mechanism for two types of CDs using laser-VFD processing. (a) MWCNTs reaching the end of the jet feed, instantly and drop-wise separate from the solvent. (b) Non-uniform distribution of defects (highlighted in red dots) on the MWCNTs generated in the mixing syringe.

There are a number of reasons for generating two types of emissions for the CDs, as summarised in Figure S9. We note that MWCNTs dispensed in the syringe pump in aqueous  $\text{H}_2\text{O}_2$  using a magnetic stirrer, prior to injecting into the VFD, showed significantly higher  $I_D/I_G$  ratio (1.34) compared with as received material (1.19) (Fig. S1) which is indicative of more defects. However, any oxidation inside the mixing syringe prior to delivery to the VFD tube is likely to be random, because of the bundling of the material (Fig. S1b), resulting in a non-uniform distribution of defects on the MWCNTs (Fig. S10).

Oxidation will also occur from the progressive interaction or chemisorption between the MWCNTs and free hydroxyl radicals ( $\text{HO}\cdot$ ) generated by the NIR laser, with the shear stress in the VFD possibly resulting in bending of the MWCNTs, like that established for SWCNTs,<sup>2</sup> and hypothesised for the slicing of MWCNTs, encouraging further oxidation by attack of C-C bonds under strain, and the high mass transfer in the dynamic thin film in the VFD.<sup>2</sup> Reaction with  $\text{HO}\cdot$  can lead to disrupting the  $\pi$ -electron network of the CNTs structure, cracking and unrolling, which can also be facilitated by increasing the temperature.<sup>5</sup> In the present case, the NIR laser will result in heating of the nanotubes, with the heat rapidly dissipated under high mass transfer conditions.

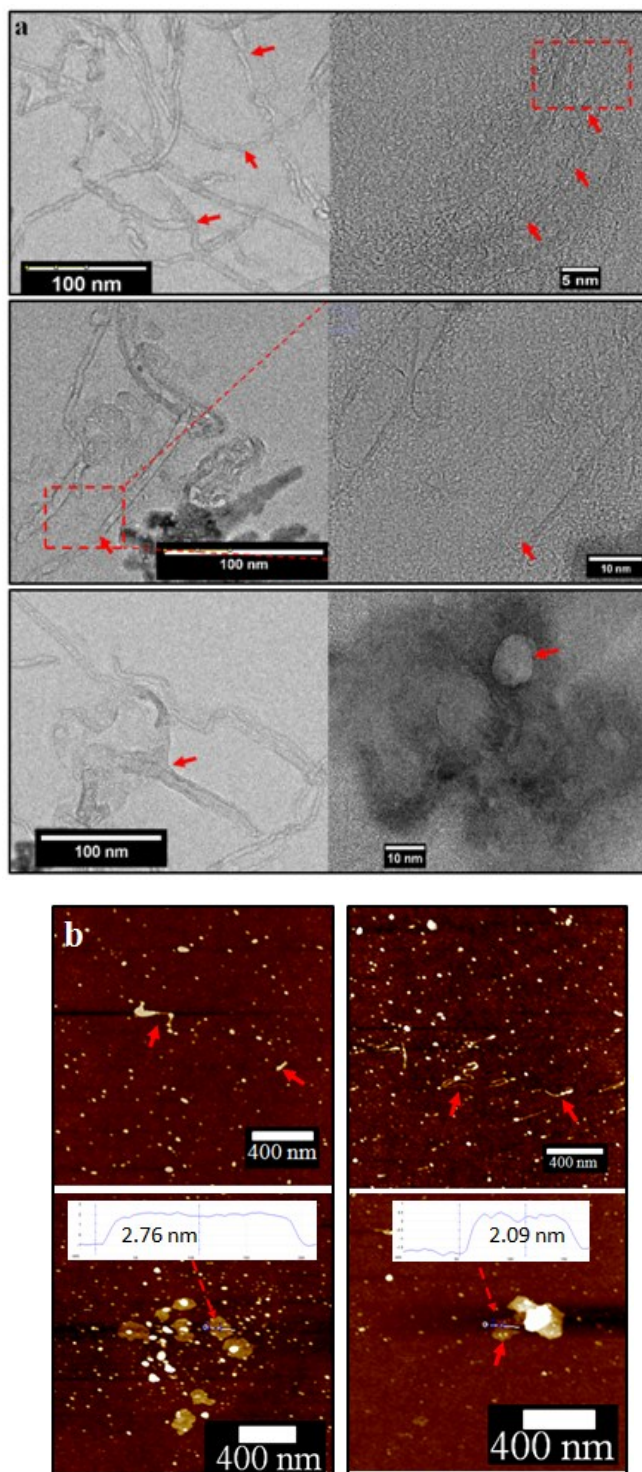


**Fig. S11** TEM, HRTEM and AFM images of the sediment of laser-VFD processed MWNCT - 7500 rpm at 0.1 mg/mL with a flow rate of 0.45 mL/min. Disrupted side walls, ruptured and shortened CNTs are highlighted with red arrows. (a) TEM and HRTEM. (b) AFM

Nanosized-holes are evident with the formation of lighter (fewer graphene layers) and darker regions (multiplied graphene layers), indicating degradation of multilayered graphene post sidewall rupture. HRTEM images of a poorly crystalline MWCNT exhibiting imperfections along the nanotube surface.

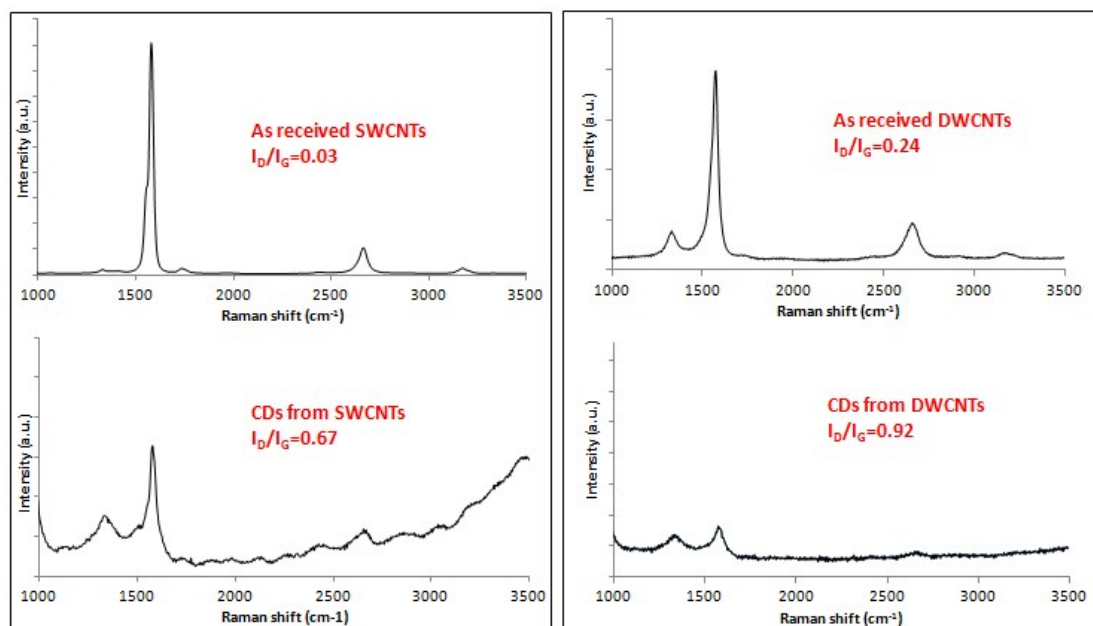
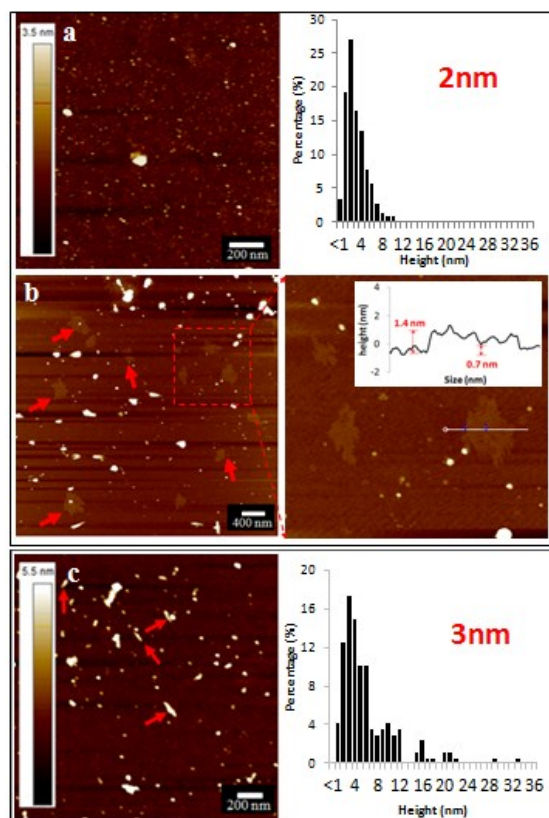


**Fig. S12** (a) AFM and the height distribution plot of as processed SWCNTs under the optimized condition of laser-VFD. (b) AFM of fragmented graphene sheets observed from as-processed SWCNTs sediment, as highlighted by red arrows. (c) AFM and height distribution plot of as-processed DWCNTs under the optimized conditions for laser-VFD processing. Short nanotubes are highlighted.

Double-walled carbon nanotubes (DWCNTs, CAS 308068-56-6) were purchased from Carbon Allotropes and single-walled carbon nanotubes (SWCNTs, CO#2023) purchased from Carbon Solution, Inc.

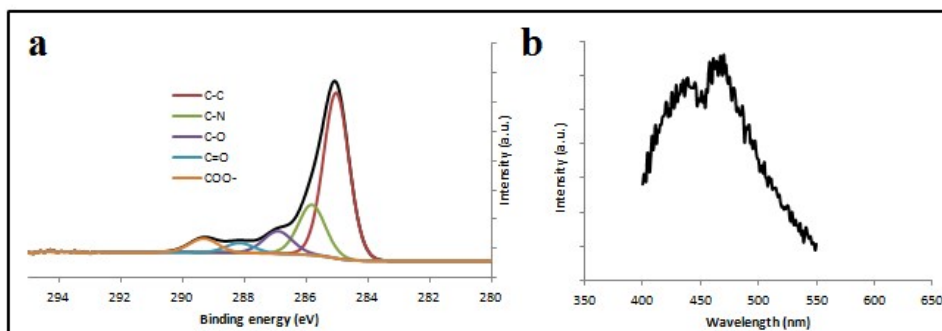


**Fig. S13.** (a) XPS of CDs dried by mixing with ammonia hydroxide and heating at 60°C in small scales. (b) PL of aqueous ammonia hydroxide dried CDs redispersed in MilliQ water.

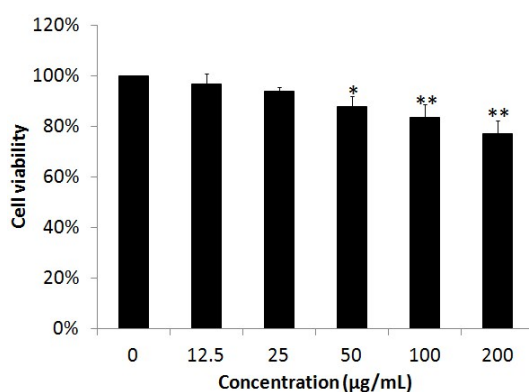


**Fig. S14.** Cell viability of skin fibroblast cells incubated with various concentrations of CDs for 24 h. Data are presented as mean±SD. Treatment significantly different from the solvent control at  $P<0.05$  were presented as \* and  $P<0.01$  as \*\*.

**Cell cultures and toxicity.** The cytotoxicity of the samples was evaluated by MTT assay. Briefly, skin fibroblast CRL2076 cells were cultured in Iscove's Modified Dulbecco's medium (IMDM) supplemented with 10% fetal bovine serum, 1% penicillin, and 1% streptomycin under a constant temperature of 37°C, 95% air and 5% CO<sub>2</sub> humidified conditions. The cells were harvested by trypsin/EDTA solution and were resuspended in fresh complete medium before plating.  $1 \times 10^5$  skin fibroblast cells were seeded in a 96 well plate and cultured for 24 h. After the medium was removed, cells were treated with CDs at different concentrations of 0, 12.5, 25, 50, 100 and 200 µg/mL for additional 24 h at 37°C. Then the medium was removed and cells were washed thoroughly with phosphate buffer saline (PBS) three times. Thereafter, the cells were treated with 0.5 mg/mL MTT followed by 37 °C incubation for 4 h whereupon 80 µL of 20% (w/v) sodium dodecyl sulfate (SDS) in 0.02 M HCl was added to each well to dissolve the formazan crystals formed. The plates were kept in dark at room temperature for 17 h. The absorbance of the formazan product was measured at 570 nm with a reference wavelength of 630 nm on µQuant Automatic Spectrophotometer (Bio-TEK instruments, NSW, Australia). At concentrations ranging from 12.5 to 50 µg/mL, more than 90% cell viability was achieved and the cellular morphology was maintained post-treatment. These results revealed that a low dose of CDs had good bio-compatibility and low toxicity.

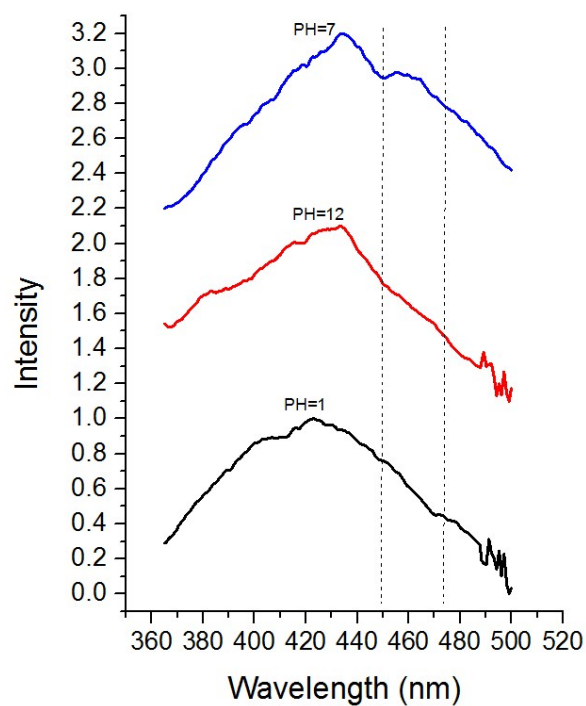


**Fig. S15.** PL emission spectra of CDs excited at 377 nm under acidic, neutral and basic conditions. Emissive peak at 460 nm under neutral conditions disappeared when adjusted to either acidic or basic pH.

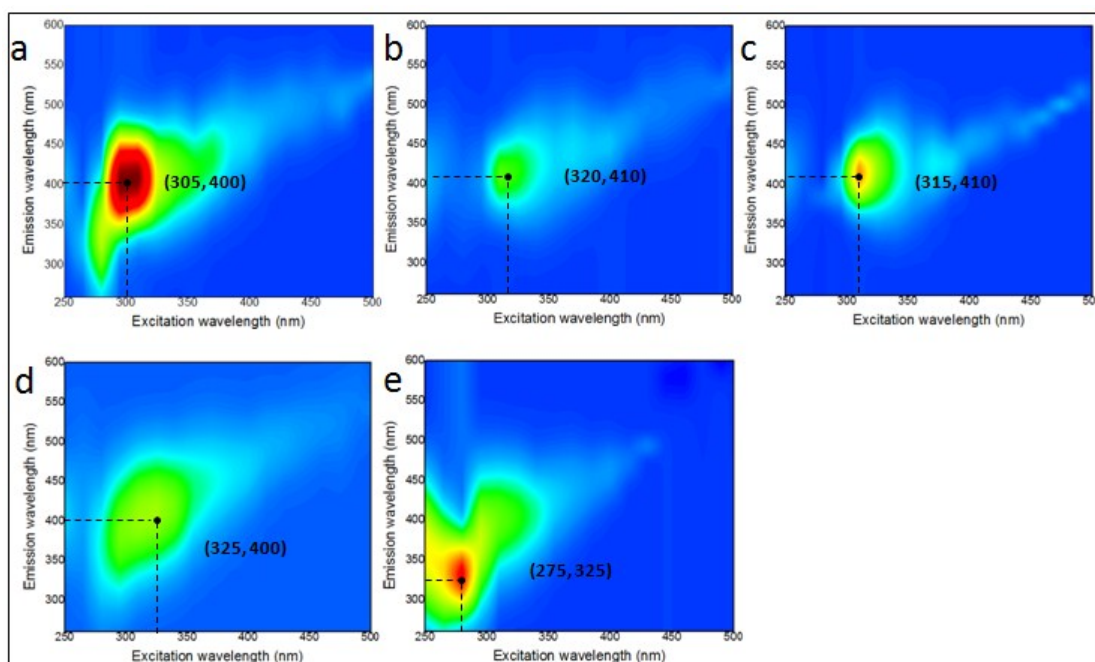


**Fig. S16.** (a) through molecular sieve only (b) through molecular sieve and magnesium sulphate at 1:1 (c) 1:2 (d) 1:3 (e) 1:4

## References

1. J. H. Lehman, M. Terrones, E. Mansfield, K. E. Hurst and V. Meunier, *Carbon* 2011, **49**, 2581-2602.
2. K. Vimalanathan, J. R. Gascooke, I. Suarez-Martinez, N. A. Marks, H. Kumari, C. J. Garvey, J. L. Atwood, W. D. Lawrance and C. L. Raston, *Sci.Rep.* 2016, **6**, 1-6.
3. J. Dilag, H. Kobus, Y. Yu, C. T. Gibson and A. V. Ellis, *Polym. Int.* 2015, **64**, 884-891.
4. B. De, N. Karak, *RSC Adv.* 2013, **3**, 8286-8290.
5. Wang, H. Shan, R. H. Hauge, M. Pasquali and R. E. Smalley, *J. Phy. Chem. B* 2007, **111**, 1249-1252.